RESEARCH ARTICLE

Air-loaded Gas Vesicle Nanoparticles Promote Cell Growth in Three-dimensional Bioprinted Tissue Constructs

Salwa Alshehri[1,2†], Ram Karan[3†], Sarah Ghalayini[1∞], Kowther Kahin[1], Zainab Khan[1], Dominik Renn[3], Sam Mathew[3], Magnus Rueping[3,4*], Charlotte A. E. Hauser[1,5*]

[1]Laboratory for Nanomedicine, Division of Biological and Environmental Science and Engineering, King Abdullah University of Science and Technology, 23955 Thuwal, Kingdom of Saudi Arabia
[2]Department of Biochemistry, Faculty of Science, University of Jeddah, Jeddah, Saudi Arabia
[3]KAUST Catalysis Center, Division of Physical Sciences and Engineering, King Abdullah University of Science and Technology, 23955 Thuwal, Kingdom of Saudi Arabia
[4]Institute for Experimental Molecular Imaging, University Clinic, RWTH Aachen University, Forckenbeckstrasse 55, D52074 Aachen, Germany
[5]Computational Bioscience Research Center, King Abdullah University of Science and Technology, Thuwal 23955-6900, Kingdom of Saudi Arabia
[∞]McGovern Medical School, Houston, TX, USA & The University of Texas MD Anderson Cancer Center UTHealth Graduate School of Biomedical Sciences, Houston, TX, USA.
[†]*These authors contributed equally to this work*
[∞]*Current affiliation*

Abstract: Three-dimensional (3D) bioprinting has emerged as a promising method for the engineering of tissues and organs. Still, it faces challenges in its widespread use due to issues with the development of bioink materials and the nutrient diffusion barrier inherent to these scaffold materials. Herein, we introduce a method to promote oxygen diffusion throughout the printed constructs using genetically encoded gas vesicles derived from haloarchaea. These hollow nanostructures are composed of a protein shell that allows gases to permeate freely while excluding the water flow. After printing cells with gas vesicles of various concentrations, the cells were observed to have increased activity and proliferation. These results suggest that air-filled gas vesicles can help overcome the diffusion barrier throughout the 3D bioprinted constructs by increasing oxygen availability to cells within the center of the construct. The biodegradable nature of the gas vesicle proteins combined with our promising results encourage their potential use as oxygen-promoting materials in biological samples.

Keywords: Three-dimensional bioprinting; Gas vesicles; *Halobacterium*; *Haloferax*; Tissue engineering

*Correspondence to: Charlotte A. E. Hauser, Laboratory for Nanomedicine, Division of Biological and Environmental Science and Engineering, King Abdullah University of Science and Technology, 23955 Thuwal, Kingdom of Saudi Arabia; charlotte.hauser@kaust.edu.sa; Magnus Rueping, KAUST Catalysis Center, Division of Physical Sciences and Engineering, King Abdullah University of Science and Technology, 23955 Thuwal, Kingdom of Saudi Arabia; magnus.rueping@kaust.edu.sa

Received: February 10, 2022; **Accepted:** March 16, 2022; **Published Online:** June 1, 2022

Citation: Alshehri S, Karan R, Ghalayini S, *et al*., 2022, Air-loaded Gas Vesicle Nanoparticles Promote Cell Growth in Three-dimensional Bioprinted Tissue Constructs. *Int J Bioprint,* 8(3):489. http://doi.org/10.18063/ijb.v8i3.489

1. Introduction

Human organs are defined by their complex, functional organization of diverse, specialized cells, and tissues[1]. The rising incidence rates of disease and injury leading to organ failure have led to increased demand for tissue and organ transplants. This growing demand has given rise to tissue engineering, whereby scaffolds, cells, and biologically active molecules are combined to assemble functional constructs. The goal is to develop constructs capable of restoring, improving, or maintaining damaged tissues and organs[2]. Of the many methods to generate these functional three-dimensional (3D) structures, 3D bioprinting is the most promising due to its ability to produce complex, scalable

tissue constructs[3,4]. The printing of these cellularized structures through the precise layering of cell-laden bioinks is accomplished using material jetting bioprinting (inkjet, microvalve, acoustic, and laser-assisted bioprinting), material extrusion bioprinting, and vat polymerization bioprinting (stereolithography, digital light processing, and two-photon polymerization)[5-13]. While each printer has its advantages over the others, there remain many challenges to face before this technology can be translated into clinical practice, regardless of the printer setup[14].

Two of the most significant issues with 3D bioprinting are identifying suitable bioinks and ensuring adequate nutrient supply to the cells[15-20]. While a great deal of effort has been focused on developing novel biomaterial candidates, it has been much harder to find a solution to address the diffusion barrier associated with the printed construct. The diffusion gradient is an inherent result of the nature of the bioink scaffolding material, which hinders the migration of nutrients, ranging from growth factors to oxygen, to the center. This diffusion barrier must be overcome as delivering these nutrients ensures the cells' survival, proliferation, and differentiation.

As such, oxygen-releasing biomaterials have been explored as a means of promoting its diffusion throughout the construct. Most of the oxygen-releasing biomaterials developed so far involve scaffolds integrated with peroxides and fluorinated compounds in the form of liquids or solid micro- and nano-particles[21,22]. Although early reports of these materials are promising, they all require the insertion of materials that do not occur naturally within the human body[23-25]. This introduces additional uncertainty about the fate of these materials as they lack the inherent biodegradability of proteins, for example. To this end, we propose an alternate solution to promote oxygen diffusion using gas vesicle nanoparticles (GVNPs). Gas vesicles are hollow gas-filled proteinaceous intracellular organelles common to many species of bacteria and archaea[26]. In nature, gas vesicles promote floatation and the availability of oxygen in the microbial cell[27]. These cylindrical- or spindle-shaped organelles have canonical ends and vary in size depending on the organism[28,29]. Over the years, GVNPs have drawn interest in biotechnological and biomedical applications. This includes traditional nanoparticle applications as drug delivery systems and other applications based on their unique physical properties. One group, in particular, the Shapiro group at Caltech, has found that their sound scattering properties and ability to produce harmonic ultrasound signals make GVNPs especially useful as contrast agents and molecular sensors for ultrasound and magnetic resonance[30-35].

In this study, we developed a new, efficient system for haloarchaeal *Haloferax volcanii* gas vesicle expression that utilizes a combination of attributes to facilitate cheaper and faster GVNP production at yields high enough to be suitable for bioreactor scale[30,36]. To improve cell growth by promoting the diffusion of oxygen, gas vesicles were printed homogeneously throughout the constructs. The bioprinting experiments were conducted with our novel 3D bioprinting system using our ultra-short peptide hydrogel[37-41]. The printability of peptide bioinks and biocompatibility with various cell types was tested[42,43].

As gas vesicles have been reported to promote cell activity in cell culture[44], this work aims to see if those findings can be extended to attain better outcomes in 3D bioprinting. The biocompatibility of the gas vesicles was tested with human embryonic kidney cells in both two-dimensional (2D) and 3D cell cultures. In addition, the printability of the gas vesicles was assessed to ensure that the nanoparticles are capable of withstanding the shear stress involved in the printing process. The bioink and scaffolding material used throughout this study was IK_6 self-assembling peptide. Once the printability and biocompatibility of the gas vesicles were established, the cell viability and morphology of cells printed with and without gas vesicles were assessed. The results are promising and suggest that the 3D printing of gas vesicles may positively affect cell activity for up to 7 days when printed together.

2. Materials and methods

2.1. Materials

The self-assembling peptide IK_6 (Ac-ILVAGK-NH2) was custom synthesized by Bachem AG (Budendorf, Switzerland). Human embryonic kidney cells (HEK293) were purchased from American Type Culture Collection (ATCC; USA). Cells were cultured in medium Dulbecco's modified Eagle's medium-high glucose (DMEM-HG; Gibco Thermo Fisher Scientific, USA). T175 or T75 cell culture flasks and 96- and 48-well plates were purchased from Corning, USA. *Halobacterium* sp. NRC-1 was obtained from Carolina Biological Supply (Burlington, NC, USA) and cultured in CM^+ medium containing 4.3M NaCl and trace metals at 42°C with shaking as previously described[45]. *H. volcanii* H1895 and its corresponding vector pTA963 were kindly provided by Dr. Thorsten Allers (Institute of Genetics, School of Biology, University of Nottingham, Queen's Medical Centre, Nottingham, UK). *H. volcanii* and derivatives were cultured in the Hv-YPC medium at 45°C with shaking as previously described[46,47]. For solid media, 2% (w/v) agar was added. The CellTiter-Glo® luminescent 3D cell viability assay kit, LIVE/DEAD® Viability/Cytotoxicity kit and Actin Cytoskeleton/Focal Adhesion Staining kit were purchased from Promega, USA, Life Technologies™, USA, and Sigma-Aldrich, USA, respectively.

2.2. Engineering and expression of gas vesicles in *H. volcanii*

Superfolder Green Fluorescent Protein (sfGFP) synthetic gene (IDT, Leuven, Belgium) was codon-

optimized using the java codon adaptation online tool JCat for *Halobacterium* sp. (strain NRC-1/ATCC 700922/JCM 11081)[48]. The gas vesicle operon from *Halobacterium* sp. NRC-1 was amplified from the genome using polymerase chain reaction (PCR) and cloned with sfGFP via *Fsp*AI-*Hpa*I and *Hpa*I-*Bam*HI using the Gibson Assembly Cloning Kit into pTA963 to generate the pTA963_sfGFP_GVNPs expression plasmid (**Table 1**). The construct was validated by restriction digestion using *Fsp*AI, *Hpa*I, and *Bam*HI, PCR amplification, and DNA sequencing. Gas vesicles containing the vector were transformed into *H. volcanii* H1895 using the PEG/EDTA method[49].

2.3. Culturing and gas vesicle preparation

The processes for producing and culturing gas vesicles were performed as previously described[27,30,47]. *H. volcanii* lawns or floating cells were lysed osmotically with phosphate-buffered saline (PBS) solution (137 mM NaCl, 2.7 mM KCl, 10 mM sodium phosphate dibasic, and 2 mM potassium phosphate monobasic [pH 7.4]) containing 10 mM $MgSO_4$ and 20 μg/mL of DNase I (Sigma-Aldrich, USA). The cell lysate suspension was incubated for 1 h at 37°C before overnight centrifugation at 60× *g* in a swinging bucket rotor in an Allegra X-15R centrifuge (Beckman Coulter, CA, USA) to accelerate floatation of the gas vesicles. Intact gas vesicles were collected and re-suspended in PBS, then floated by overnight centrifugation and harvested again. This floatation procedure was repeated until a white, milky suspension of gas vesicles was obtained. Gas vesicle concentration was quantified via NanoDrop 2000 spectrophotometer (Thermo Scientific, Waltham, MA, USA) by measuring a small sample of gas vesicles broken by sonicating for several minutes.

2.4. Hydrogel preparation

The ultrashort peptide IK_6 (Ac-ILVAGK-NH2) used in this study was synthesized by Bachem AG (Budendorf, Switzerland) using solid-phase peptide synthesis and purified to above 95% through high-performance liquid chromatography. Amino acid and peptide content analyses were performed. The lyophilized peptide powders were first dissolved in Milli-Q water and mixed by vortexing for 30 s to obtain a homogenous solution. Then, ×10 PBS was added to the peptide solution for a final concentration of ×1. Gelation occurred within a few minutes at 8 mg/mL peptide concentration.

2.5. 2D cell culture

HEK293 cells were purchased from ATCC (USA). Cells were cultured in DMEM-HG, supplemented with 10% (v/v) fetal bovine serum (FBS) and 1% penicillin/streptomycin (PS; Gibco) at 37°C with 5% CO_2. The cells were subcultured with trypsin at approximately 80% confluence. The culture media were changed every 2 – 3 days. Cells at passages 6 – 8 were encapsulated for 3D culture and monolayer culture.

2.6. 3D cell culture

HEK293 cells were cultured in 75T flasks and incubated in a CO_2 incubator maintained at 37°C with 5% CO_2. Culture media were replaced every 48 h until the cells reached 80% confluency. Confluent cells were subcultured, and cells at passages 6 – 8 were used for the study. For the 3D culture, the peptide was sterilized by exposure to ultraviolet light for 30 min. 10,000 cells in ×2 PBS were mixed at a 1:1 ratio with peptide solution and used to prepare 100 μl of 3D construct in a 96-well plate without the addition of GVNPs to serve as a control. Different concentrations of GVNPs were obtained by mixing with PBS before adding them to form 3D samples. This allowed for the evaluation of the GVNPs effect on cell proliferation.

2.7. 3D bioprinting

16 mM of IK_6 peptide was diluted in 1 mL of MilliQ water, mixed well, and sonicated to assure a homogenous solution. Eight million cells were suspended in ×1 PBS without GVNPs (control). When printing with GVNPs, the cells were mixed with a ×1 PBS containing GVNPs at a 300 μg/ml concentration.

A custom-designed 3D bioprinter along with commercial microfluidic pumps was set up **(Figure S1)** as described in our previous publications, and a homemade dual coaxial nozzle was used for bioink extrusion[40,41,50]. Structures were printed in the shape of a rectangular prism with a length, width, and height of 10 mm, 10 mm, and 1.5 mm, respectively. Illustrated figure of the printed structure along with the printer setup is shown in **Figure 1**. To facilitate imaging, the structure was printed onto an 18 × 18 mm glass coverslip. The glass coverslip

Table 1. Oligonucleotides used in this study.

Primer	5'-3' sequence
pTA.1	GGACCTATTGCGCATATGCACCACCACCACCACCACATGCGCATAATTCAATCGATACGAGTCCCG
pTA.2	AATGCGATGGTCCAGAGGTGCGGCCGCTCTAGAACTAGTGGATCCGATCTGTGAGTGTACACCCC
*Hpa*I-*Bam*HI	TGTCTCTTCTTCCTCGTTAACGGTACCGGCGGATTCTCC
*Fsp*AI-*Hpa*I	GCGGAGAATCCGCCGGTACCGTTAACGAGGAAGAAGAGACAGAGCC

was then placed on top of a heat-bed set to 40°C to create a suitable temperature environment for the cells.

Three syringe pumps were set up to dispense homogenous gel and extrude peptide bioink through the nozzle. The first syringe pump was loaded with peptide solution and set to a flow rate of 55 µL/min. The second pump was loaded with ×7 PBS and set to a flow rate of 20 µL/min. The third pump was loaded with the cells and set to a flow rate of 20 µL/min. Three samples of the 4-layer rectangular prism were printed for each condition with a height of 1.5 mm per sample to facilitate imaging. The same procedure was conducted for samples without gas vesicles to serve as controls.

2.8. 3D cell proliferation assay

The CellTiter-Glo® luminescent 3D cell viability assay was used to assess cell proliferation in 3D hydrogels by measuring ATP production. At each time point, the kit was equilibrated at room temperature for approximately 30 min. CellTiter-Glo® Reagent equal to the volume of cell culture medium present in each well was added. The contents were mixed for 5 min to digest the hydrogels and then incubated for 30 min. After incubation, the luminescence was recorded using a plate reader (PHERAstar FS, Germany).

2.9. Live/dead staining

HEK293 cells were seeded into peptide according to the protocol described above. After one, three, and 7 days of incubation, the media was removed and replaced with PBS containing approximately 2 mM calcein AM and 4 mM ethidium homodimer-1 before incubation for 40 min. Before imaging, the staining solution was removed, and fresh PBS was added. Stained cells were imaged under an inverted confocal microscope (Zeiss LSM 710 Inverted Confocal Microscope, Germany). The percentage of living cells was obtained through analysis with ImageJ.

2.10. Cytoskeletal staining and imaging

Immunostaining was performed at each culture time point. In brief, the cells were fixed with 4% (v/v) paraformaldehyde solution for 30 min and incubated in a cold cytoskeleton buffer (3 mM $MgCl_2$, 300 mM sucrose, and 0.5% [v/v] Triton X-100 in PBS solution) for 5 min to permeabilize the cell membranes. The permeabilized cells were then incubated in blocking buffer solution (5% FBS, 0.1% (v/v) Tween-20, and 0.02% [w/v] sodium azide in PBS) for 30 min at 37°C. For F-Actin, anti-mouse IgG (whole molecule)-FITC and rhodamine-phalloidin (1:300) were added to the cells for 1 h. Further, the cells were incubated in DAPI for 5 min to counterstain the nucleus. The fluorescent dye-treated cells were observed and imaged using a laser scanning confocal microscope (Zeiss LSM 710 Inverted Confocal).

2.11. Scanning electron microscopy (SEM)

The printed samples were characterized using SEM to visualize the morphology of the peptide bioink and gas vesicles in printed samples[50]. Samples were printed on 18 × 18 mm glass coverslips and given time to solidify before dehydration by gradual immersion in increasing concentrations of 20%, 40%, 60%, 80%, and 100% (v/v) ethanol solutions for 5 min in each solution. Further dehydration in 100% ethanol solution was done by changing the absolute ethanol solution with a fresh ethanol solution twice for 5 min each, followed by a third time for 2 h. Dehydrated samples were subsequently placed into the critical point dryer (Sorvall Critical Point Drying System) for evaporation before being mounted onto SEM aluminum pin stubs with double-stick conductive carbon tape and a final sputter coating of 10 nm of iridium. Images were taken with FEI Magellan XHR SEM. This was done with a TLD detector, and imaging parameters included a current of 50 pA, a high voltage of 3.00 kV, and a working distance of 4.0 m. Biological peptide hydrogel coating cells were fixed with 2.5% (v/v) glutaraldehyde (diluted from 25%) in water overnight at 4°C, the post-

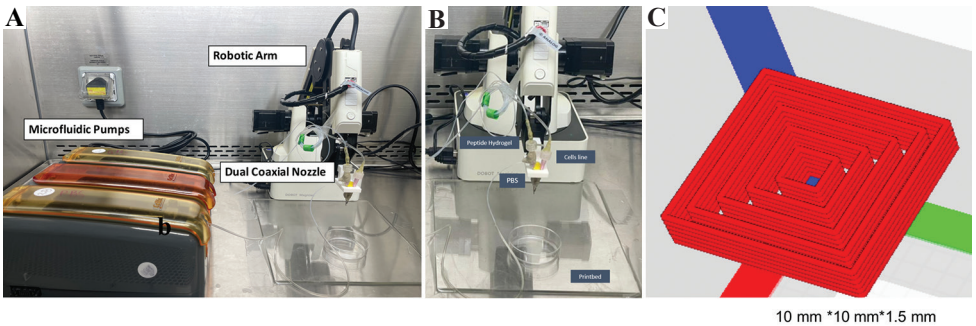

Figure 1. (A and B) Image of the 3D bioprinter setup used for experiments conducted in this study and (C) a preview of the gcode file of the printed structure with dimensions measuring 10 mm × 10 mm × 1.5 mm.

fixation was done by 1% (w/v) osmium tetroxide in 0.1 M PBS for 1 h in the dark followed by washing 3 times by ddH_2O. This was followed by serial dehydration with 10 mL of H_2O (twice), 25% ethanol, 50% ethanol, 75% ethanol, 80% ethanol, 90% ethanol, and 100% (v/v) ethanol (twice). Samples in ethanol were then critically point dried using liquid CO_2 (Sorvall Critical Point Drying System).

2.12. Statistical analysis

All experimental approaches were executed in triplicates to allow for statistical testing. Results are represented as mean ± standard deviation, $n \geq 3$. The differences observed in HEK293 cell behavior for conditions with and without GVNPs were compared. Statistical analysis was performed by a Student's *t*-test, and values with $P < 0.05$ were considered statistically significant.

3. Results and discussion

3.1. Characterization of GVNPs

Haloarchaeal GVNPs are attractive for biotechnological and biomedical applications and have already found use as drug delivery systems and contrast agents for ultrasound and magnetic resonance imaging[30-35]. While the biotechnological tools for the expression of GVNPs are now established, production so far suffers from the slow growth rates, the inconsistent induction system, and the genetic instability of the *Halobacterium* expression host. Therefore, we developed a new plasmid construct allowing fast and high-yielding GVNPs production in *H. volcanii* without the requirement of antibiotics. The completely sequenced and clean genetic background with respect to gas vesicle genes makes *H. volcanii* a suitable and attractive organism of choice for expressing *Halobacterium* GVNPs. *H. volcanii* is a nonpathogenic halophile that grows to high density in the presence of high concentrations of salt, which precludes contamination by less halophilic microorganisms[47,51].

Expression of the gas vesicle operon in *H. volcanii* led to spindle- or cylinder-shaped gas vesicles with conical tips. Transmission electron microscopy (FEI Titan CT microscope) equipped with a 4 k × 4 k CCD camera (Gatan, Pleasanton, CA, USA) and dynamic light scattering (DLS, Zetasizer Nano, Malvern Inc., Malvern, U.K.) measurements of purified gas vesicles nanoparticle suspensions range from 30 to 250 nm in width and from 40 nm to 1.5 μm in length with a mean diameter of 255 nm (**Figure 2**). The straightforward protein expression system and efficient purification process produced a substantial number of gas vesicles that can be scaled (**Figure S2**). In addition, the spindle or cylindrical shape of these GVNPs (**Figure 2**) is of particular interest in this study because the increased volume to surface area ratio allows improved gas exchange and nutrient diffusion. The size of the gas vesicles is also ideal for biomedical applications. GVNPs are small enough to fit within the pores of the fibrous extracellular matrix (ECM) while still too large to cross the blood-brain barrier and cell membrane[52].

3.2. Hexapeptide characterization

The IK_6 amphiphilic peptide was designed with a hydrophilic head group at the C terminus followed by a series of hydrophobic residues, increasing in hydrophobicity to the N terminus at the tail end of the peptide. The peptide in this study readily formed a hydrogel in PBS with the aforementioned method, and was selected for its rapid self-assembly, ease of use, and biocompatibility. As a bioink, this peptide demonstrated excellent gelling properties as it formed quickly enough to ensure the structural integrity of the construct and printed smoothly to avoid clumping or inconsistencies as some other materials have. We have previously reported fibrous peptide network formation, characterizing the structures with circular dichroism (CD) and X-ray diffraction[53]. The peptide IK_6 form similar network as recently described self-assembling ultrashort tera peptide compound[54,55]. In this case, the peptide was characterized with SEM after printing with our printing system **(Figure 3, Figure S3)**. This imaging showed evidence of the hydrogel's formation of a fibrous network present throughout the construct. These morphological characteristics are similar to those observed in hydrogel samples prepared manually. The samples prepared for imaging were at a concentration of approximately 16 mM, which is the minimum gelation concentration, and this concentration of peptide was used for the remainder of the printing experiments with the cells and GVNPs. This ensured that the printing in subsequent experiments occurred smoothly and consistently, and further highlights both the versatility of our printing system and the strong case for the use of ultrashort self-assembling peptide as bioink material.

3.3. Effect of GVNPs on cell viability in 3D construct

Halobacterium sp. NRC-1 gas vesicle cytotoxicity was assessed through the 2D culture of HEK cells in a previous study[30]. The results showed nearly 100% cell viability even at the highest concentrations of GVNPs tested, approximately 500 μg/mL[30]. Cytotoxicity of gas vesicles expressed in *H. volcanii* was assessed in this work by testing cell growth and proliferation in 2D culture (**Figure S4**) and 3D culture with varying concentrations of GVNPs.

Bright-field microscopy imaging and cell viability (live/dead assay) were performed to examine the HEK

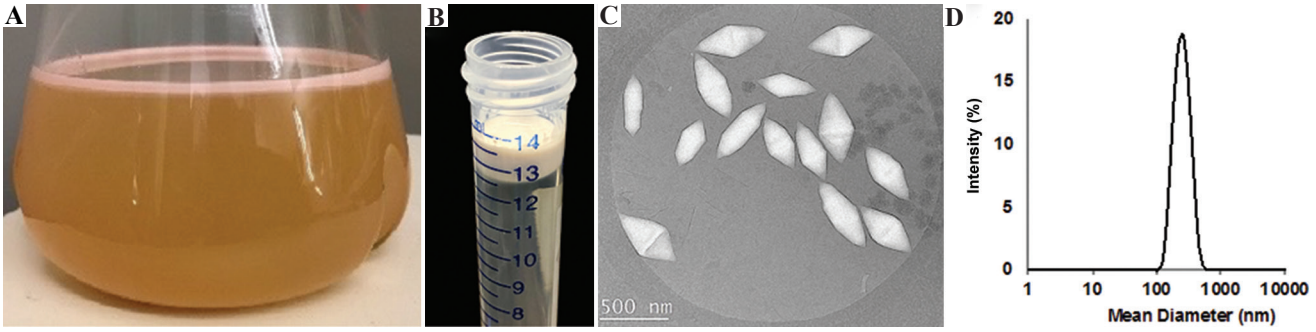

Figure 2. Characterized gas vesicles. (A) *Haloferax volcanii* cells grown in liquid culture and left to stand, buoyant cells floating at the top. (B) Pure white gas vesicles floating at the top. (C) Intact gas vesicles imaged with transmission electron microscopy. (D) DLS particle size distribution profile of purified gas vesicles.

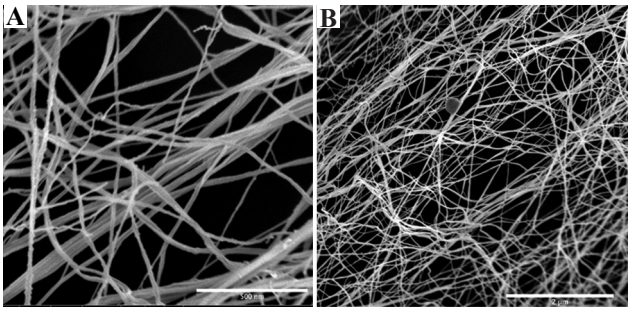

Figure 3. Morphological characterization of the printed peptide scaffold by scanning electron microscopy. Condensed fibers of IK_6 hydrogels at a concentration of 16 mM. Images were obtained at ×200,000 (A) and ×50,000 (B) magnification.

cells in 3D constructs cultured with GVNPs, and the images are shown below in **Figure 4A-D** through 3D. Cell proliferation was also quantified with the CellTiter-Glo Assay, and these results are shown in **Figure 4E**. An increase in cell activity was observed from day 1 to day 7. When compared to the control group, the cells cultured with GVNPs showed significantly increased proliferation. Furthermore, cell proliferation increases with increasing concentrations of GVNPs. Significant difference was found in the proliferation of cells cultured with 750 μg/mL GVNPs at days 1 and 7 compared to the control.

In this study, the biocompatibility of gas vesicles expressed in *H. volcanii* was confirmed by 3D culture of HEK 293 cells with various concentrations of GVNPs. Qualitative and quantitative assessment concerning cell growth, morphology, and proliferation is provided **(Figure 4)**, demonstrating that the gas vesicles have no associated toxicity at all tested concentrations. These findings are consistent with those of other studies where no adverse effects of GVNPs have been observed[35,56-59].

3.4. 3D Bioprinting process

Before conducting experiments with GVNPs, various shapes were printed using IK_6 peptide to optimize printing parameters. After tuning several parameters, including peptide and PBS flow rates, the rapid gelation of the IK_6 peptide facilitated smooth and consistent extrusion of the bioink, thus achieving a more refined and stable construct of 10 mm in height (**Figure 5A and B**). Our previous study further reports on the bioprintability, structure fidelity, and cell viability of IK_6 peptide[60]. Moreover, to assure the stability of the bioprinted construct during the incubation period, the construct fidelity was observed over time for several weeks (**Figure 5C and D**). After 8 weeks, the construct maintained structure and hold shape, thus confirming the high structure fidelity of the IK_6 peptide.

Several experiments were conducted to ensure the suitability of the gas vesicles for bioprinting and to determine the optimal printing parameters. The previous studies have found that gas vesicles are relatively weak and their strength varies depending on the organism and strain from which they are derived[27,29]. As such, the first of our printing experiments focused on ensuring that the gas vesicles could withstand the stress of the printing process. This was assessed via SEM imaging to compare the morphology of the printed gas vesicles to those that were not printed. The imaging of 3D printed gas vesicles (**Figure 5F and G**) also revealed that nearly all of the gas vesicles remained intact, thereby providing further evidence of the strength of halophilic gas vesicles and suggesting potential applications of gas vesicles for biomedical applications. This builds on the previous work reporting that the recombinant GVNPs were observed to be stable for several months at room temperature and at elevated temperatures of around 50°C, with little to no degradation[35].

Another attractive feature for biotechnological and biomedical applications is the fragile nature of the S-layer cell walls, which can be easily lysed upon addition of water, releasing cellular proteins and reducing the cost of protein purification[61,62]. Further, we displayed the sfGFP on the GVNPs surface and demonstrated the application of GVNPs as imaging

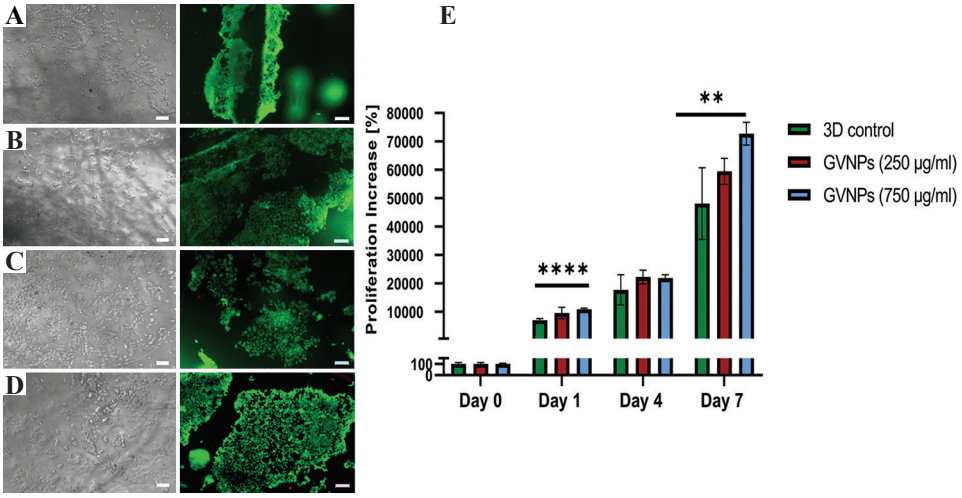

Figure 4. Cell proliferation in 3D constructs. (A-D) Bright-field microscopy images and fluorescence images (live cells in green, dead cells in red) of HEK cells in 3D constructs after 1 day of culture at varying GVNP concentrations (A: Control, B: 250 µg/mL, C: 500 µg/mL, D: 750 µg/mL). Scale bar: 100 µm. (E) The percentage of cell proliferation rate normalized against the initial time point day 0 was shown as mean ± SD ($n = 6$). $^{**}P < 0.01$, $^{****}P < 0.0001$.

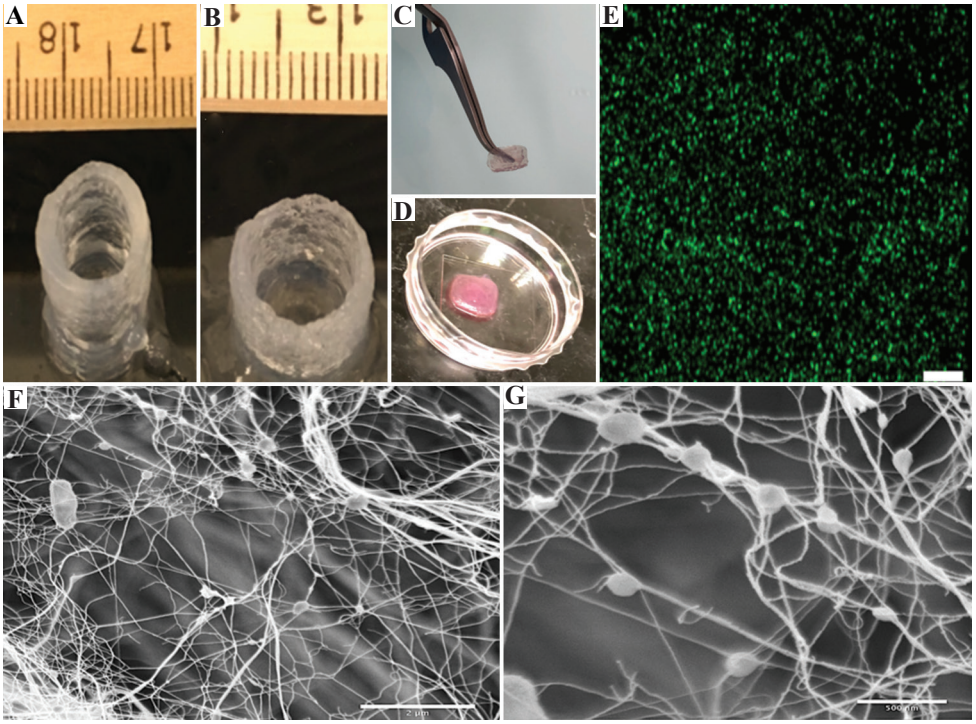

Figure 5. (A) Image of 1 cm cylinder printed with IK_6 peptide on day 1, and (B) image of the same construct after 8 weeks, (C and D) images showing a 3D bioprinted sample undergoing preparations for imaging, (E) confocal imaging of the engineered sfGFP gas vesicles within the 3D printed sample, scale bar: 2 µm, (F and G) SEM imaging of printed GVNPs. Morphological characterization of the printed peptide scaffold with GVNPs by SEM. Images were obtained at ×35,000 (F) and ×100,000 (G) magnification.

tools and oxygen carriers as well as protein display and delivery vehicle (**Figure 5E**). This was done to ensure a homogenous distribution throughout the construct and was studied using fluorescent gas vesicle particles engineered with sfGFP.

3.5. Influence of GVNPs on the viability of bioprinted cells

The HEK 293 cells were 3D printed, and the cell viability was studied at three different time points. The results are shown in **Figure 6A and B**, and live/dead cell staining

and quantified cell viability data are included. In samples analyzed 24 h after bioprinting, about 85.8 ± 4.8% of cells were observed to be alive in the control group without GVNPs, while an increase in viability to 89.7 ± 3.7 was found in samples with GVNPs at this time point. A significant increase was found in cell viability when measured 4 and 7 days after printing with GVNPs from 83.4 ± 4.6 to 92.6 ± 3.7 on day 4 and 91.3± 3.9 to 96.4± 2.1 on day 7 with $P = 0.0005$ and 0.009, respectively.

The imaging results in **Figure 6A** show that the GVNPs did not affect the morphology of the HEK293 cells. An earlier study reported that the addition of GVNPs to cells in 2D culture was associated with an increase in cell activity[44]. Our results (**Figure 6A and B**) suggest that the cells printed with GVNPs showed better viability than the cells printed alone. As the GVNPs constitute the thin protein-membrane and the gases inside and are permeable to gases in the environment, the effect is likely due to the gas permeability of the protein shell. One way through which this can occur is by promoting the availability of oxygen to the cells as the oxygen is allowed to diffuse from within the gas vesicles to the surrounding environment. This increased oxygen availability may render the environment more similar to favorable *in vivo* conditions, thereby promoting cell survival. Another possibility could be that nearby GVNPs enable cells to clear waste or other species within the environment more rapidly. Byproducts of cellular respiration include CO_2, so the permeability of the GVNP shell coupled with the concentration gradient of the different gases in the system may have promoted the diffusion of CO_2 away from the cells.

3.6. Morphological study of bioprinted cells

Cell aggregates formed within gels after printing, and their actin cytoskeletons and nuclei were stained. The growth of the cell aggregates is tracked over 7 days and visible in **Figure 7A**. The growing size of the cellular aggregates over time is evidence for cell proliferation. These aggregates increase in diameter, as shown in **Figure 5**. This finding is consistent with the previous study; after 7 days of culture, HEK 293 become dense in structure with multiple cells aggregate up to 140 μm in width[63]. Moreover, electron microscopy imaging was performed to visualize the GVNPs in the gel construct after printing. These images depicting the GVNPs in the environment surrounding the cells 2 and 8 days after printing are shown in **Figure 7B**. This is in contrast with the lack of gas vesicles present in the imaged control samples.

As we aimed to test the potential for these protein-based nanostructures in promoting the growth of printed cells, it was crucial to preserve cell viability, morphology, and function after printing[64-67]. Therefore, we optimized the 3D bioprinting parameters for HEK 293 cells and incorporated the GVNPs into the 3D construct by adjusting syringe pump flow rates, inner diameters of the nozzle, printing speed, and layer height to mitigate such effect. The notion that cell growth and death are very strongly affected by the extracellular environment has been well documented in the literature[68]. The ECM is crucial to tissue engineering, as it dictates cellular morphology and guides the connections between cells and the site of interactions. Together, the ECM architecture and its composition affect cell growth, connection, differentiation, and adhesion. Our results indicate that the GVNPs were able to incorporate within the peptide fibers. The gas vesicles were also able to stay within the extracellular environment for at least 8 days, possibly increasing the porosity of the gel constructs, thereby allowing more medium and nutrients to penetrate the center.

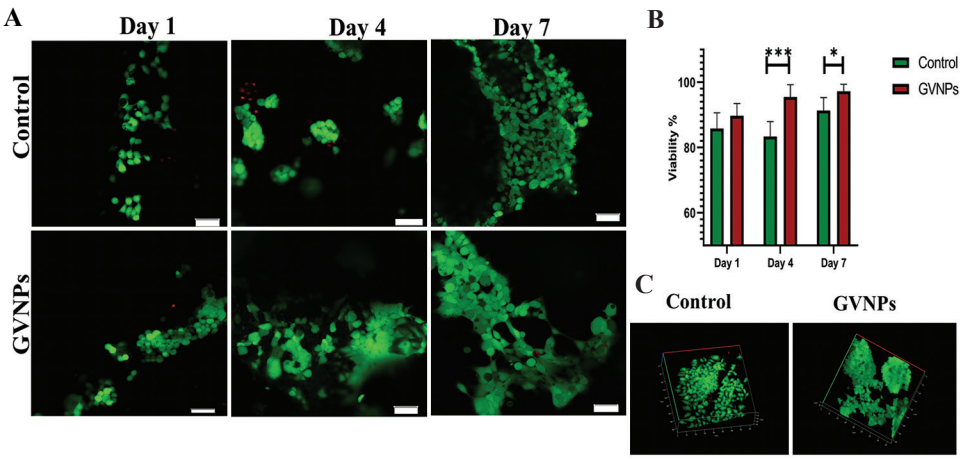

Figure 6. (A) Live/dead staining images for the printed cells with and without GVNPs at days 1, 4, and 7 after printing scale bar 100 μm. (B) The quantitative analysis of cell viability by ImageJ for the 6 different images. (C) Morphology and 3D distribution of the cells within printed constructs after 7 days. $*P < 0.05$, $***P < 0.001$.

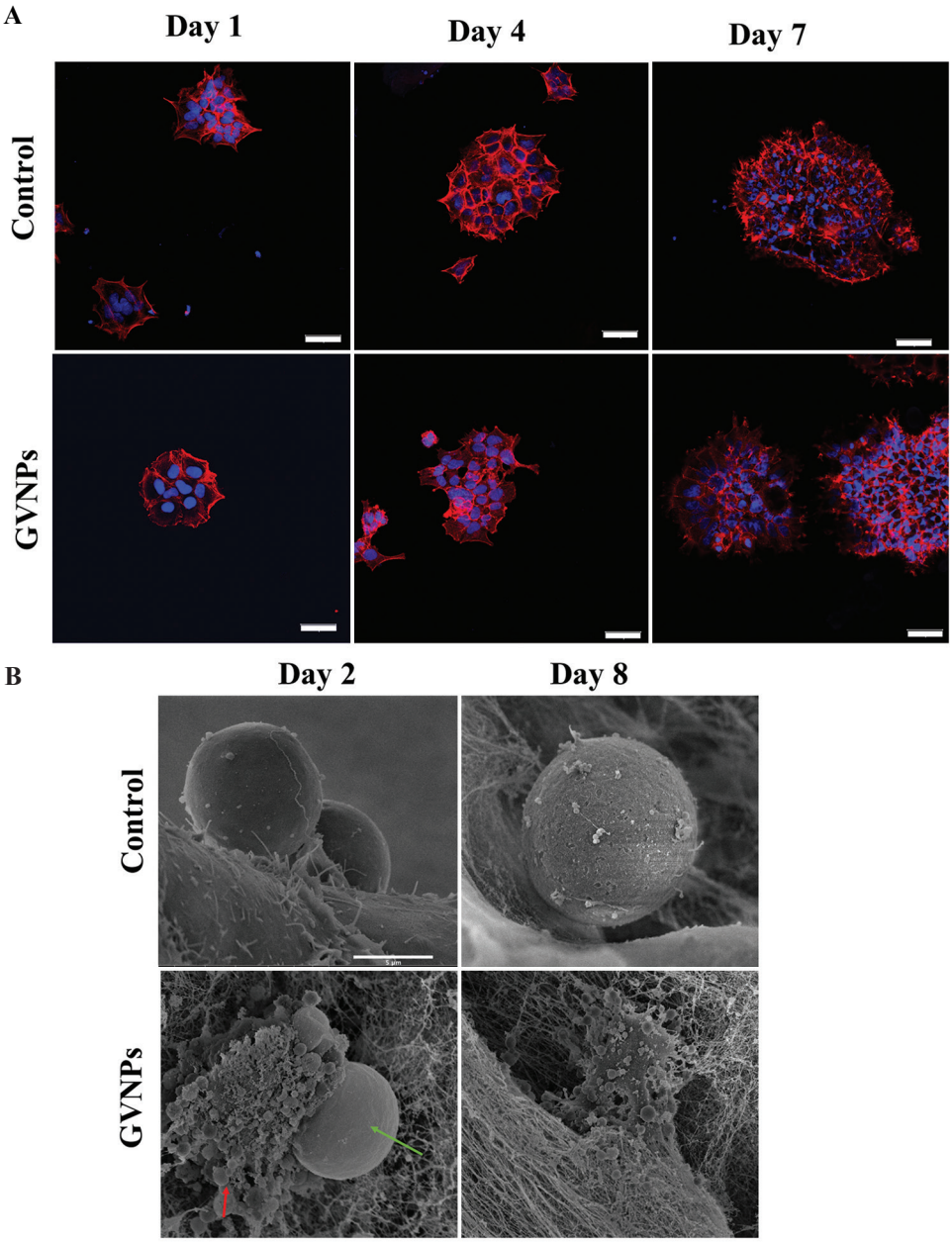

Figure 7. Cell aggregate morphology. (A) Fluorescence confocal microscopy images taken 1, 4, and 7 days after printing (nucleus shown in blue, F-actin shown in red). Scale bar: 50 μm. (B) Electron microscope images of printed cells with and without GVNPs. Red arrow indicates NPs and the green arrow indicates the cell.

4. Conclusion

Gas vesicles have many advantages over other nanostructures that make them excellent materials for applications in medicine. These gas-filled stable protein nanostructures are uniquely well suited for bioengineering. Many previous studies have explored GVNPs applications in therapeutics, antigen display, and vaccine production[36,69,70]. Our study establishes the use of genetically encoded gas vesicles to promote cell viability within 3D printed constructs, thereby bringing 3D bioprinting one step closer to printing large tissues and organs. Future studies will build on the *in vitro* proofs of the concept presented in this study to test the effect of loading the gas vesicles with gas oxygen concentrations that more closely mimic those of different *in vivo* settings and test their efficacy in promoting cell viability in larger constructs.

Our research will further advance 3D bioprinting methods and the development of a gas vesicle expression system in mammalian cells. Our findings that gas vesicles can withstand the stress associated with the bioprinting

process and positively influence cell viability suggest that this method can promote the survival of cells within 3D printed constructs. Gas vesicles can be used as a bridge to promote cell viability between construct formation and vascularization in the future.

Acknowledgments

The authors thank Dr. Thorsten Allers for generously providing us with *H. volcanii* H1895 and its corresponding vector pTA963. We thank the research intern, Alvin Huang, for protein nanoparticle production and purification assistance. The research reported in this publication was supported by funding from King Abdullah University of Science and Technology and University of Jeddah.

Conflict of interest

The authors declare that they have no conflicts of interest.

Author contributions

C.A.E.H. and M.R. conceived, directed the study and planned the experiments. R.K. designed and constructed the GVNP expression system and performed the GVNP characterization with D.R. and S.M. S.A. and S.G. performed the biocompatibility study. Z.K and K.K designed the 3D printing system and performed the bioprinting. S.A. carried out the SEM and confocal imaging. S.A. prepared the manuscript with assistance from R.K. and S.G. All authors provided input on the study and experimental design, analysis, and manuscript.

References

1. Cui H, Nowicki M, Fisher JP, *et al.*, 2017, 3D Bioprinting for Organ Regeneration. *Adv Healthc Mater*, 6:1601118. https://doi.org/10.1002/adhm.201601118
2. Khademhosseini A, Langer R, 2016, A decade of Progress in Tissue Engineering. *Nat Protoc*, 11:1775–81. https://doi.org/10.1038/nprot.2016.123
3. Matai I, Kaur G, Seyedsalehi A, *et al*., 2020, Progress in 3D Bioprinting Technology for Tissue/Organ Regenerative Engineering. *Biomaterials*, 226:119536. https://doi.org/10.1016/j.biomaterials.2019.119536
4. Ng WL, Chua CK, Shen YF, 2019, Print me an Organ! Why we are not there yet. *Prog Polym Sci*, 97:101145. https://doi.org/10.1016/j.progpolymsci.2019.101145
5. Bishop ES, Mostafa S, Pakvasa M, *et al.*, 2017, 3-D Bioprinting Technologies in Tissue Engineering and Regenerative Medicine: Current and Future Trends. *Genes Dis*, 4:185–95. https://doi.org/10.1016/j.gendis.2017.10.002
6. Murphy SV, Atala A, 2014, 3D Bioprinting of Tissues and Organs. *Nat Biotechnol*, 32:773–85. https://doi.org/10.1038/nbt.2958
7. Seol YJ, Kang HW, Lee SJ, *et al.*, 2014, Bioprinting Technology and its Applications. *Eur J Cardio Thorac Surg*, 46:342–8. https://doi.org/10.1093/ejcts/ezu148
8. Li X, Liu B, Pei B, *et al.*, 2020, Inkjet Bioprinting of Biomaterials. *Chem Rev*, 120:10793–833. https://doi.org/10.1021/acs.chemrev.0c00008
9. Ng WL, Lee JM, Yeong WY, *et al.*, 2017, Microvalve-based Bioprinting-process, Bio-inks and Applications. *Biomater Sci*, 5:632–47.
10. Jentsch S, Nasehi R, Kuckelkorn C, *et al.*, 2021, Multiscale 3D Bioprinting by Nozzle-Free Acoustic Droplet Ejection. *Small Methods*, 5:2000971. https://doi.org/10.1002/smtd.202000971
11. Dou C, Perez V, Qu J, *et al.*, 2021, A State-of-the-Art Review of Laser-Assisted Bioprinting and its Future Research Trends. *ChemBioEng Rev*, 8:517–34. https://doi.org/10.1002/cben.202000037
12. Fu Z, Naghieh S, Xu C, *et al*., 2021, Printability in Extrusion Bioprinting. *Biofabrication*, 13:033001. https://doi.org/10.1088/1758-5090/abe7ab
13. Ng WL, Lee JM, Zhou M, *et al*., 2020, Vat Polymerization-based Bioprinting-process, Materials, Applications and Regulatory Challenges. *Biofabrication*, 12:022001. https://doi.org/10.1088/1758-5090/ab6034
14. Ravnic DJ, Leberfinger AN, Koduru SV, *et al*., 2017, Transplantation of Bioprinted Tissues and Organs: Technical and Clinical Challenges and Future Perspectives. *Ann Surg*, 266:48-58. https://doi.org/10.1097/sla.0000000000002141
15. Hauser CA, Zhang SG, 2010, Designer Self-assembling Peptide Nanofiber Biological Materials. *Chem Soc Rev*, 39:2780–90. https://doi.org/10.1039/b921448h
16. Chen C, Bang S, Cho Y, *et al*., 2016, Research Trends in Biomimetic Medical Materials for Tissue Engineering: 3D Bioprinting, Surface Modification, Nano/Micro-technology and Clinical Aspects in Tissue Engineering of Cartilage and Bone. *Biomater Res*, 20:10. https://doi.org/10.1186/s40824-016-0057-3
17. Visconti RP, Kasyanov V, Gentile C, *et al*., 2010, Towards Organ Printing: Engineering an Intra-organ Branched Vascular Tree. *Expert Opin Biol Ther*, 10:409–20. https://doi.org/10.1517/14712590903563352
18. Kolesky DB, Homan KA, Skylar-Scott MA, *et al*., 2016, Three-dimensional Bioprinting of Thick Vascularized

Tissues. *Proc Natl Acad Sci*, 113:3179–84. https://doi.org/10.1073/pnas.1521342113

19. Zhang B, Luo Y, Ma L, *et al*., 2018, 3D Bioprinting: An Emerging Technology Full of Opportunities and Challenges. *Biodes Manuf*, 1:2-13. https://doi.org/10.1007/s42242-018-0004-3
20. Zhang YS, Yue K, Aleman J, *et al*., 2017, 3D Bioprinting for Tissue and Organ Fabrication. *Ann Biomed Eng*, 45:148–63. https://doi.org/10.1007/s10439-016-1612-8
21. Suvarnapathaki S, Wu X, Lantigua D, *et al*., 2019, Breathing Life into Engineered Tissues Using Oxygen-releasing Biomaterials. *NPG Asia Mater*, 11:65. https://doi.org/10.1038/s41427-019-0166-2
22. Erdem A, Darabi MA, Nasiri R, *et al*., 2020, 3D Bioprinting of Oxygenated Cell-Laden Gelatin Methacryloyl Constructs. *Adv Healthc Mater*, 9:1901794. https://doi.org/10.1002/adhm.201901794
23. Pedraza E, Coronel MM, Fraker CA, *et al*., 2012, Preventing Hypoxia-induced Cell Death in Beta Cells and Islets Via Hydrolytically Activated, Oxygen-generating Biomaterials. *Proc Natl Acad Sci U S A*, 109:4245–4250. https://doi.org/10.1073/pnas.1113560109
24. McQuilling JP, Sittadjody S, Pendergraft S, *et al*., 2017, Applications of Particulate Oxygen-generating Substances (POGS) in the Bioartificial Pancreas. *Biomater Sci*, 5:2437–47. https://doi.org/10.1039/c7bm00790f
25. Ward KR, Huvard GS, McHugh M, *et al*., 2013, Chemical Oxygen Generation. *Respir Care*, 58:184–95. https://doi.org/10.4187/respcare.01983
26. Pfeifer F, 2015, Haloarchaea and the Formation of Gas Vesicles. *Life*, 5:385–402.
27. DasSarma S, Karan R, DasSarma P, *et al*., 2013, An Improved Genetic System for Bioengineering Buoyant Gas Vesicle Nanoparticles from Haloarchaea. *BMC Biotechnol*, 13:112. https://doi.org/10.1186/1472-6750-13-112
28. Kunth M, Lu GJ, Witte C, *et al*., 2018, Protein Nanostructures Produce Self-Adjusting Hyperpolarized Magnetic Resonance Imaging Contrast through Physical Gas Partitioning. *ACS Nano*, 12:10939–48. https://doi.org/10.1021/acsnano.8b04222
29. Pfeifer F, 2012, Distribution, Formation and Regulation of Gas Vesicles. *Nat Rev Microbiol*, 10:705–15. https://doi.org/10.1038/nrmicro2834
30. Andar AU, Karan R, Pecher WT, *et al*., 2017, Microneedle-Assisted Skin Permeation by Nontoxic Bioengineerable Gas Vesicle Nanoparticles. *Mol Pharm*, 14:953–8. https://doi.org/10.1021/acs.molpharmaceut.6b00859
31. Lu GJ, Chou LD, Malounda D, *et al*., 2020, Genetically Encodable Contrast Agents for Optical Coherence Tomography. *ACS Nano*, 14:7823–31. https://doi.org/10.1021/acsnano.9b08432
32. Szablowski JO, Bar-Zion A, Shapiro MG, 2019, Achieving Spatial and Molecular Specificity with Ultrasound-targeted Biomolecular Nanotherapeutics. *Acc Chem Res*, 52:2427–34. https://doi.org/10.1021/acs.accounts.9b00277
33. Lu GJ, Farhadi A, Szablowski JO, *et al*., 2018, Acoustically Modulated Magnetic Resonance Imaging of Gas-filled Protein Nanostructures. *Nat Mater*, 17:456–63. https://doi.org/10.1038 s41563-018-0023-7
34. Lakshmanan A, Farhadi A, Nety SP, *et al*., 2016, Molecular Engineering of Acoustic Protein Nanostructures. *ACS Nano*, 10:7314–22. https://doi.org/10.1021/acsnano.6b03364
35. DasSarma P, Negi VD, Balakrishnan A, *et al*., 2014, Haloarchaeal Gas Vesicle Nanoparticles Displaying *Salmonella* SopB Antigen Reduce Bacterial Burden when Administered with Live Attenuated Bacteria. *Vaccine*, 32:4543–9. https://doi.org/10.1016/j.vaccine.2014.06.021
36. Balakrishnan A, DasSarma P, Bhattacharjee O, *et al*., 2016, Halobacterial nano vesicles displaying murine bactericidal permeability-increasing protein rescue mice from lethal endotoxic shock. *Sci Rep*, 6:1–11. https://doi.org/10.1038/srep33679
37. Loo Y, Lakshmanan A, Ni M, *et al*., 2015, Peptide Bioink: Self-assembling Nanofibrous Scaffolds for Three-dimensional Organotypic Cultures. *Nano Lett*, 15:6919–25. https://doi.org/10.1021/acs.nanolett.5b02859
38. Loo Y, Hauser CA, 2015, Bioprinting Synthetic Self-assembling Peptide Hydrogels for Biomedical Applications. *Biomed Mater*, 11:014103. https://doi.org/10.1088/1748-6041/11/1/014103
39. Sundaramurthi D, Rauf S, Hauser C, 2016, 3D Bioprinting Technology for Regenerative Medicine Applications. *Int J Bioprint*, 2:78. https://doi.org/10.18063/IJB.2016.02.010
40. Khan Z, Kahin K, Rauf S, *et al*., 2019, Optimization of a 3D Bioprinting Process Using Ultrashort Peptide Bioinks. *Int J Bioprint*, 5:173. https://doi.org/10.18063/ijb.v5i1.173
41. Kahin K, Khan Z, Albagami M, *et al*., 2019, Development of a Robotic 3D Bioprinting and Microfluidic Pumping System

for Tissue and Organ Engineering, Microfluidics, BioMEMS, and Medical Microsystems XVII. International Society for Optics and Photonics, 108750Q.

42. Rauf S, Susapto HH, Kahin K, *et al*., 2020, Self-assembling Tetrameric Peptides Allow *In Situ* 3D Bioprinting under Physiological Conditions. *J Mater Chem B*, 9:1069–81. https://doi.org/10.1039/D0TB02424D
43. Susapto HH, Alhattab D, Abdelrahman S, *et al.*, 2021, Ultrashort Peptide Bioinks Support Automated Printing of Large-Scale Constructs Assuring Long-Term Survival of Printed Tissue Constructs. *Nano Lett*, 21:2719–29. https://doi.org/10.1021/acs.nanolett.0c04426
44. Sundararajan A, Ju LK, 2006, Use of Cyanobacterial Gas Vesicles as Oxygen Carriers in Cell Culture. *Cytotechnology*, 52:139–49. https://doi.org/10.1007/s10616-007-9044-9
45. DasSarma S, Fleischmann E, Rodriguez-Valera F, 1995, Media for halophiles. In: Robb FT, Place AR, Sowers KR, Schreier HJ, DasSarma S, Fleischmann ME, editors. Archaea: A Laboratory Manual. Vol. 1. Cold Spring Harbor, NY: Cold Spring Harbor Laboratory Press, p225–30.
46. Strillinger E, Grötzinger SW, Allers T, *et al.*, 2016, Production of Halophilic Proteins Using *Haloferax volcanii* H1895 in a Stirred-tank Bioreactor. *Appl Microbiol Biotechnol*, 100:1183–95. https://doi.org/10.1007/s00253-015-7007-1
47. Grotzinger SW, Karan R, Strillinger E, *et al.*, 2018, Identification and Experimental Characterization of an Extremophilic Brine Pool Alcohol Dehydrogenase from Single Amplified Genomes. *ACS Chem Biol*, 13:161–70. https://doi.org/10.1021/acschembio.7b00792
48. Grote A, Hiller K, Scheer M, *et al.*, 2005, JCat: A Novel Tool to Adapt Codon Usage of a Target Gene to its Potential Expression Host. *Nucleic Acids Res*, 33(Web Server issue):W526–31. https://doi.org/10.1093/nar/gki376
49. Dyall-Smith M, 2008, The Halohandbook-Protocols for Haloarchaeal Genetics, Version 7.0. Bathurst, NSW, Australia. Available from: https://haloarchaea.com/wp-content/uploads/2018/10/Halohandbook_2009_v7.3mds.pdf
50. Ghalayini S, Susapto HH, Hall S, *et al.*, 2019, Preparation and Printability of Ultrashort Self-assembling Peptide Nanoparticles. *Int J Bioprint*, 5:239. https://doi.org/10.18063/ijb.v5i2.239
51. Akal AL, Karan R, Hohl A, *et al*., 2019, A Polyextremophilic Alcohol Dehydrogenase from the Atlantis II Deep Red Sea Brine Pool. *FEBS Open Bio*, 9:194–205. https://doi.org/10.1002/2211-5463.12557
52. Silva IC, Delgado AB, Silva PH, *et al.*, 2018, Focused ultrasound and Alzheimer's disease A systematic review. *Dement Neuropsychol*, 12:353–9. https://doi.org/10.1590/1980-57642018dn12-040003
53. Hauser CA, Deng R, Mishra A, *et al.*, 2011, Natural Tri- to Hexapeptides Self-assemble in Water to Amyloid Beta-type Fiber Aggregates by Unexpected Alpha-helical Intermediate Structures. *Proc Natl Acad Sci U S A*, 108:1361–6. https://doi.org/10.1073/pnas.1014796108
54. Alshehri S, Susapto HH, Hauser CA, 2021, Scaffolds from Self-Assembling Tetrapeptides Support 3D Spreading, Osteogenic Differentiation, and Angiogenesis of Mesenchymal Stem Cells. *Biomacromolecules*, 22:2094–106. https://doi.org/10.1021/acs.biomac.1c00205
55. Gustavo Ramirez-Calderon H H S a C A E H, 2021, Delivery of Endothelial Cell-Laden Microgel Elicits Angiogenesis in Self-Assembling Ultrashort Peptide Hydrogels *In Vitro*. *ACS Appl Mater Interfaces*, 13:29281–92. https://doi.org/10.1021/acsami.1c03787
56. Stuart ES, Morshed F, Sremac M, *et al*., 2001, Antigen Presentation Using Novel Particulate Organelles from Halophilic Archaea. *J Biotechnol*, 88:119–28. https://doi.org/10.1016/S0168-1656(01)00267-X
57. DasSarma P, Negi V, Balakrishnan A, *et al*., 2015, Haloarchaeal Gas Vesicle Nanoparticles Displaying *Salmonella* Antigens as a Novel Approach to Vaccine Development. *Proc Vaccinol*, 9:16. https://doi.org/10.1016/j.provac.2015.05.003
58. Sremac M, Stuart ES, 2008, Recombinant Gas Vesicles from *Halobacterium* sp. Displaying SIV Peptides Demonstrate Biotechnology Potential as a Pathogen Peptide Delivery Vehicle. *BMC Biotechnol*, 8:9. https://doi.org/10.1186/1472-6750-8-9
59. Stuart ES, Morshed F, Sremac M, *et al.*, 2004, Cassette-based Presentation of SIV Epitopes with Recombinant Gas Vesicles from Halophilic Archaea. *J Biotechnol*, 114:225–37. https://doi.org/10.1016/j.jbiotec.2004.01.005
60. Khan Z, Kahin K, Melle F, *et al*., 2019, Assessing the Bioprintability of Self-Assembling Peptide Bioinks in Terms of Structure Fidelity and Cell Viability. 9th International Conference on Advances in Applied Science and Environmental Technology, p8-14.
61. Vogler M, Karan R, Renn D, *et al*., 2020, Crystal Structure and Active Site Engineering of a Halophilic gamma-Carbonic Anhydrase. *Front Microbiol*, 11:742.

https://doi.org/10.3389/fmicb.2020.00742

62. Karan R, Mathew S, Muhammad R, *et al*., 2020, Understanding High-salt and Cold Adaptation of a Polyextremophilic Enzyme. *Microorganisms*, 8:1594. https://doi.org/10.3390/microorganisms8101594
63. Graham AD, Olof SN, Burke MJ, *et al*., 2017, High-resolution Patterned Cellular Constructs by Droplet-based 3D Printing. *Sci Rep*, 7:7004. https://doi.org/10.1038/s41598-017-06358-x
64. Nair K, Gandhi M, Khalil S, *et al*., 2009, Characterization of Cell Viability during Bioprinting Processes. *Biotechnol J*, 4:1168–77. https://doi.org/10.1002/biot.200900004
65. Yu Y, Zhang Y, Martin JA, *et al*., 2013, Evaluation of Cell Viability and Functionality in Vessel-like Bioprintable Cell-laden Tubular Channels. *J Biomech Eng*, 135:91011. https://doi.org/10.1115/1.4024575
66. Yan KC, Nair K, Sun W, 2010, Three Dimensional Multi-scale Modelling and Analysis of Cell Damage in Cell-encapsulated Alginate Constructs. *J Biomech*, 43:1031–8. https://doi.org/10.1016/j.jbiomech.2009.12.018
67. Jakab K, Norotte C, Marga F, *et al*., 2010, Tissue Engineering by Self-assembly and Bio-printing of Living Cells. *Biofabrication*, 2:022001. https://doi.org/10.1088/1758-5082/2/2/022001
68. De Jong OG, Van Balkom BW, Schiffelers RM, *et al*., 2014, Extracellular Vesicles: Potential Roles in Regenerative Medicine. *Front Immunol*, 5:608. https://doi.org/10.3389/fimmu.2014.00608
69. DasSarma S, DasSarma P, 2015, Gas Vesicle Nanoparticles for Antigen Display. *Vaccines*, 3:686–702. https://doi.org/10.3390/vaccines3030686
70. Dutta S, DasSarma P, DasSarma S, *et al*., 2015, Immunogenicity and Protective Potential of a *Plasmodium* spp. Enolase Peptide Displayed on Archaeal Gas Vesicle Nanoparticles. *Malaria J*, 14:406. https://doi.org/10.1186/s12936-015-0914

Publisher's note